Mechanism of HflX-mediated recycling of *E. coli* ribosome studied by time-resolved cryo-EM

Sayan Bhattacharjee[1,#], Xiangsong Feng[1,#], Suvrajit Maji[1], Zuben P Brown[1,2], Joachim Frank[1*].

[1]Biochemistry and Molecular Biophysics & Biological Sciences, Columbia University, New York, USA
[2] Current address: Thermo Fisher Scientific, Oregon, USA
[#] These authors contributed equally
* Corresponding author

Recycling of stalled, translationally inactive ribosomes is one of the response mechanisms underlying resistance to environmental stress. HflX, a bacterial GTPase overexpressed upon heat shock and exposure to antibiotics, catalyzes the splitting of stalled ribosomes[1-6]. Due to its rapid rate, an attempt to follow this process in real time at room temperature requires time-resolved techniques on the scale of tens of milliseconds[1]. Here we show the time course of the splitting of *E. coli* 70S ribosome by HflX in the presence of GTP using time-resolved cryo-EM with a microfluidic device. We report the structures of three short-lived intermediate states within 140 ms of mixing 70S ribosomes with HflX and GTP. Binding of HflX and GTP hydrolysis induces breakage of multiple intersubunit bridges and opening of the 70S ribosome in a clamshell-like manner as the 30S subunit rotates around an axis with hinges formed by the remaining intersubunit bridges B3 and B7a. At 900 ms virtually all ribosomes are dissociated, while HflX remains bound to the 50S subunit. Our analysis of the structural intermediates not only allows the mechanism of HflX-catalyzed ribosome splitting to be followed in molecular detail but also to shed light on related processes: recycling of the post-termination complex by RRF/EF-G.

In *Escherichia coli* (*E. coli*), GTPase ***H**igh **f**requency of **l**ysogenization **X*** (HflX), a universally conserved protein for prokaryotes, acts as a ribosome-splitting factor during the heat shock response[1,6,7]. Recent studies revealed that HflX splits antibiotic-stalled 70S ribosomes from pathogenic *Mycobacterium abscessus* and nonpathogenic *Mycobacterium smegmatis*[3], dissociates hibernating homodimeric 70S into 50S and 30S subunits in *Staphylococcus aureus*[8], regulates hypoxia-induced replication arrest in *Mycobacterium bovis*[2], binds to the 50S subunit of *Chlamydophila pneumoniae*[5] and *Sulfolobus solfataricus*[9], and acts as a gatekeeper by regulating the manganese level in *E. coli*[4]. Thus, HflX is a remarkably multi-functional protein with a common mode of action: the splitting of stalled 70S ribosomes into its subunits in a wide range of prokaryotes. Given that HflX shares structural similarities with Release Factors 3 (RF3) and Ribosome Recycling Factor (RRF) on the ribosome and that it occupies the A-site tRNA position on the 50S subunit similar to the release factor's GGQ motif–containing loop[1], the time-dependent structural study on the progressive splitting of the 70S by HflX could reveal the mechanism of ribosome recycling, as well. Furthemore understanding the detailed structural mechanism of splitting could benefit the development of a new class of broad-spectrum antibiotics.

E. coli HflX consists of four domains: N-terminal domain (NTD), GTP binding domain (GBD), C-terminal domain (CTD), and helical linker domain (HLD)[1,10]. The cryo-EM structure of the HflX-50S complex in the presence of GMP-PNP, a non-hydrolysable GTP analog, reveals that the HLD and NTD of HflX bind to the peptidyl transferase center in a way similar to RRF, causing significant conformational changes in the intersubunit bridge B2a (h44:H69),

and thereby promoting the dissociation of the 70S ribosome[1]. According to the dissociation kinetics measured by light scattering, the rate of dissociation of vacant ribosomes (without tRNA and mRNA) by HflX in the presence of GMP-PNP or GTP is $k_{obs\ HflX\text{-}GMP\text{-}PNP} = 0.22 \pm 0.003\ s^{-1}$ and $k_{obs\ GTP} = 0.2 \pm 0.002\ s^{-1}$, respectively[1]. This rapid rate makes the progress of ribosome splitting by HflX difficult to study at room temperature using the conventional blotting method of cryo-EM sample preparation[11]. So far, the only HflX-bound ribosome structure is the 50S-GNP-PNP complex, which was solved at a resolution of 4.5 Å and considered to represent the state immediately after subunit dissociation[1]. Thus, due to the absence of any structures of short-lived reaction intermediates the mechanism of HflX-mediated ribosome splitting has remained unknown. To capture on-pathway intermediates in an in vitro reaction of HflX-GTP with 70S ribosomes, we used time-resolved cryo-EM[12-16]. We were able to capture three intermediate states, which allowed us to follow the recycling process of 70S ribosomes catalyzed by HflX at room temperature.

HflX acts on the 70S ribosome in a nucleotide-dependent way, and light scattering analysis revealed that the rate of ribosome splitting by HflX-GTP (with GTP and RRF-EF-G-GTP the rates are $k_{obs\ HflX\text{-}GTP} = 0.002\ s^{-1}$ and $k_{obs\ RRF\text{-}EF\text{-}G\text{-}GTP} = 0.005\ s^{-1}$, respectively[6,17]) is very similar to the rate of ribosome dissociation by the combined action of RRF and EF-G-GTP[6,17]. The fraction of ribosomes split into subunits at room temperature within a reaction time of 140 ms is close to 50%, according to our earlier TR cryo-EM experiment on *E. coli* ribosome recycling in the presence of RRF, EF-G, and GTP[15]. In view of these findings, we aimed our TR cryo-EM study at a 140 ms reaction time

and added both shorter (10 ms and 25 ms) time points and one longer one (900 ms) toward the reaction's completion. We mixed 70S ribosomes with the HflX-GTP complex in our mixing-spraying TR cryo-EM apparatus using different PDMS-based microfluidic chips (Methods and Extended Data Fig. 2). As in our previous TR studies[15,16], 3D classification was performed on the entire, pooled dataset. The 3D classification produced seven distinct classes, which we characterized by examination of the corresponding reconstructed density maps. (Here "rotated" and "nonrotated" refers to the presence or absence of intersubunit rotation[18]): (1) rotated 70S without HflX ($r70S_{noHflX}$); (2) non-rotated 70S without HflX ($nr70S_{noHflX}$); (3) 70S-like intermediate-I with HflX ($i70S_{HflX}$-I); (4) 70S like-intermediate-II with HflX ($i70S_{HflX}$-II); (5) 70S-like intermediate-III with HflX ($i70S_{HflX}$-III); (6) 50S with HflX ($50S_{HflX}$); and (7) 30S (Methods and Extended Data Fig. 5, and 6). The splitting reaction kinetics of the 70S ribosome, as evaluated by following the number of particles obtained upon 3D classifications from 10 ms to 900 ms, is found to follow a similar roughly exponential behavior as reported from dissociation kinetics measured by light scattering[1] (Fig 1G). Furthermore, we noticed a rapid increase in the number of free 30S particles from 140 ms to 900 ms, which implies that the final separation of the subunits commences not earlier than with state $i70S_{HflX}$-III (Fig. 1G).

The three HflX-containing intermediates and $50S_{HflX}$ -- four of the seven 3D classes we found -- were selected for additional structural analysis (Methods and Extended Data Fig. 5, and 6A-E). Furthermore, focused 3D classification and subsequent reconstruction of HflX binding regions from each of the resulting class reconstructions yielded high-resolution density maps

for four states of HflX: (1) HflX-I, (2) HflX-II, (3) HflX-III, and (4) HflX-IV (Extended Data Fig. 5). Refinement on the three i70S$_{HflX}$ class reconstructions yielded high-resolution on-pathway intermediates i70S$_{HflX}$-I, i70S$_{HflX}$-II, and i70S$_{HflX}$-III (resolutions are indicated in Extended Data Fig. 7 and Extended Data Table 2). The kinetics of the reaction can be followed from the histogram of particle counts in the respective classes (Fig. 1G). Intermediates i70S$_{HflX}$-I, i70S$_{HflX}$-II, and i70S$_{HflX}$-III are each dominated by contributions from 10 ms, 25 ms, and 140 ms, respectively. Comparison of the atomic models obtained for these intermediates with one another and with the apo-70S revealed that the opening and splitting of the 70S ribosome occurs in the following steps:

First, the ribosome opens slightly to accommodate the initial binding of HflX in i70S$_{HflX}$-I (Fig. 1A). Using the tool previously developed[19] we find that in this first intermediate, the 30S subunit has rotated by 5.9° around an axis (Axis I) that passes through the intersubunit bridges B1b, B2a, B3, and B4 (Extended Data Fig. 8A, D, G, and 8J-K), and this rotation has moved protein S6 of 30S into close vicinity to protein L2 of 50S (Fig. 1E-F). Apparently, the insertion of HflX along with the prying apart of the 70S ribosome and the rotation of the 30S subunit are facilitated by the increased backbone entropy of L2 in i70S$_{HflX}$-I compared to apo-70S (the predicted binding and solvation free energies between L2 and S6 are same for apo-70S and i70S$_{HflX}$-I; see Methods and Extended Data Table 3) since we find indication of disorder: the density of L2 is not resolved well in i70S$_{HflX}$-I (Fig. 1F) compared to all its other manifestations in apo-70S, i70S$_{HflX}$-II and i70S$_{HflX}$-III (Fig. 1E, and 2D-F). Comparison of the 50S subunit in i70S$_{HflX}$-I and apo-70S shows that H69 has moved by 6.7 Å, apparently by a push by HflX since fitting the model of

HflX to apo-70S reveals a steric clash with H69 (Fig. 1H, I). In i70S$_{HflX}$-I HflX is blurred, indicating motion-induced heterogeneity (Extended Data Fig. 5).

Going from this first intermediate to i70SHflX-II and i70SHflX-III we observe stepwise rotations, by 7.9° and 8.2°, respectively, of the 30S subunit around a new axis (Axis II) passing through intersubunit bridges B3 and B7a, which are both located along helix h44 (Fig. 1B-C, and Extended Data Fig. 8B-C, 8E-F, 8H-I, and 8J-K). In the first step of rotation around this new axis, protein S6 of the 30S subunit moves away from protein L2 (Fig. 2A-B, 2D-E, and Extended Data Fig. 8B, 8E, 8H, and 8J-K). This movement is enabled by a 6.5 Å pull of C1965 of H71 by the loop-helix motif (G74-V100) of HflX NTD (Fig. 3C, and Extended Data Fig. 9A-C). As a consequence bridge B3 (h44:H71) as well as bridges B7b and B7bR have become unstable (binding and solvation free energies between L2 and S6 of i70S$_{HflX}$-II decrease from corresponding apo-70S, see Extended Data Table 3). While the conformation of the 30S subunit remains the same from apo-70S to first intermediate, the change from first to second intermediate is accompanied by a rotation of the 30S subunit head by 2.1° around another axis, Axis III (Extended Figure 10A-C).

In the second step of the 30S subunit rotation around Axis II, from i70S$_{HflX}$-II to i70S$_{HflX}$-III, protein S6 has continued to move away from protein L2 (Fig. 2B-C, 2E-F, and Extended Data Fig. 8C, 8F, 8I, and 8J-K). Bridges B7b and B7bR are now entirely disrupted (no contacts found between L2 and S6 in free energy prediction, see Extended Data Table 3), allowing the flexible loop (E323-G349) of HflX's GTD to readily access the small subunit protein

S12, thus positioned to jettison the 30S subunit from the 70S ribosome (Fig. 3D).

Finally, the reconstruction of the stable 50S-HflX complex, at 3.6 Å resolution (Extended Data Fig. 11A), shows no longer any trace of density from the 30S subunit (Fig. 1D, 3A-B and Extended Data Fig. 11A, and D). This class mainly contains particles from 900 ms (Fig. 1G). The map agrees very well with the map of HflX-50S-GNP-PNP previously published[1] (Extended Data Fig. 11A-C).

Comparison of the atomic models built for the three intermediate states reveals that HflX undergoes considerable conformational and positional changes on the 70S ribosome, specifically in its CTD, HLD, and NTD (see movie 1 in Supplementary Material). The domain movements associated with the CTD and HLD match quite well with the dynamics of apo-HflX predicted from 1000 ns of molecular dynamics simulations (Extended Data Fig. 12A-C). Interestingly, the loop-helix motif (G74-V100) of NTD makes stable contact with H71 of the 50S subunit in state HflX-II (Fig. 3C, and Extended Data Fig. 9E-G).

In trying to understand the actions of HflX, we investigated the nucleotide state of GTP in the different states of HflX. At 25 ms, with exception of their NTDs, the densities of HflX in states HflX-I, HflX-II and associated GTPs are not resolved as well as they are for the other two classes, indicating mobility and preventing determination of nucleotide state (Extended Data Fig. 5). In an attempt to fit the atomic model of GTP to the corresponding densities in HflX-III and HflX-IV, we observed that the density in the region of the nucleotide site on HflX-III is a better fit for GDP·Pi than GTP or GDP

(Extended Data Fig. 9A-B) A similar matching effort resulted in a decent match of GTP to the density of HflX bound to the 50S subunit, even though the GDP state is expected to be found at this stage (Extended Data Fig. 9C-D).

Since at the 140 ms time point Pi is still associated with GDP and none of the 30S subunits have been cleaved, we conclude that the energy for the breaking of bridges B3 and B7a and the final dissociation of the 30S subunit is set free by Pi release. It is unclear without further investigation if GTP hydrolysis plays a role in the initial stages of splitting, from intermediate I to III, since it is known that HflX can perform the splitting in the absence of GTP, albeit with a slower rate[1]. The likely explanation for the observation of GTP on the 50S subunit-bound HflX molecule at 900 ms is that by that time both Pi and GDP have left and that a new GTP molecule has taken their place (Extended Data Fig. 9C-D).

With the axes and angles of 30S subunit rotation known, as well as the location of bridges relative to the axes, we were able to determine the distances between constituent residues of all intersubunit bridges. From these distances we can determine at which time points the intersubunit bridges are ruptured. According to these geometric calculations, the bridges B1a, B1b, B2a, and B2b are already broken at 10 ms. B5, B6 and B7b break within 140 ms. Finally, the last two bridges B3 and B7a, which formed the hinges of Axis II, give way between 140 ms and 900 ms. Bridge B4 (H34:S15) presents an interesting case as it behaves like a spring: its 50S constituent H34 is initially compressed in the step from apo-70S to i70SHflX-I, as HflX is accommodated within the first 10 ms, but in the next two steps (10 ms to 25 ms to 140 ms) it is extended. This

bridge finally breaks along with B3 and B7a after 140 ms (Extended Data Fig. 9H-I).

Our study leaves open the question on how HflX recognizes the stalled state of the ribosome. Here our observation of 30S subunit head rotation from apo-70S to i70SHflX-I may offer a clue. Puromysine-treated polysomes, having deacylated tRNA in the P site, display greatly enhanced HflX splitting activity, and this state was proposed as the natural substrate for HflX[1]. In this state, the ribosome is known to undergo spontaneous intersubunit rotation[20] which goes hand in hand with 30S subunit head 'swivel' rotation[21]. This would suggest that HflX initially binds to the ribosome in its rotated conformation and forces it into the unrotated conformation observed in i70SHflX-I, with residual 30S subunit head rotation.

Another interesting question is whether our findings about the time course and stepwise process of HflX-catalyzed ribosome splitting may inform us about the time course of RRF/EF-G-GTP-induced splitting of the post-termination complex. (A previous TR cryo-EM study of this process in vitro by our group[15] was unable to observe early states of subunit separation). We see two striking similarities between the two processes: (1) in RRF-bound post-termination complex[15,22], the helix-loop-helix motif of domain I approaches helix 71 within 140 ms, in a position that is similar to the position of the loop-helix motif (G74-V100) of NTD of HflX in intermediate i70S$_{HflX}$-II, similarly capable of pulling on H71 (Extended Data Fig. 9A-C and 10D-G). (2) The final dissociation of the 30S subunit occurs through an interaction of RRF domain II with protein S12, at the expense of hydrolysis of GTP associated with EF-G, in a way that is quite similar to that of the flexible loop (E323-G349) of

HflX GTD (Extended Data Fig. 10D-G). (3) A third similarity holds if our hypothesis of HflX binding to the rotated ribosome is correct since the latter is the substrate of RRF/EF-G-GTP binding, as well[23,24].

Here, we have shown how time-resolved cryo-EM can capture high-resolution structures of intermediates on-the-fly to reveal short-lived reaction intermediates that represent snapshots of an unfolding molecular mechanism. A combination of experimental and theoretical approaches has been used to study the molecular mechanism of bacterial resistance under stress. Based on our cumulative observations from the examination of the three intermediates, we propose that within 10 ms, the initial binding of HflX is followed by the stepwise clamshell-like opening of the ribosome around an axis that closely aligns with helix 44 of the 30S subunit. By the time 900 ms has elapsed, the combined dynamics of CTD (according to experimental evidence[6] and prediction from MD simulation, the CTD moves by up to 60 Å; see Extended Data Fig. 12B) and NLD enable HflX to split the 30S from the 50S subunit at the cost of energy set free by GTP hydrolysis and release of the inorganic phosphate (Fig. 4).

Given that the combined actions of RRF and EF-G promote ribosome of post-termination ribosomes and that the rate of recycling is comparable to the rate of ribosome splitting by HflX, our observed mechanism of ribosome splitting by HflX can fill in some gaps in explaining details of the general ribosome recycling mechanism.

FIGURES.

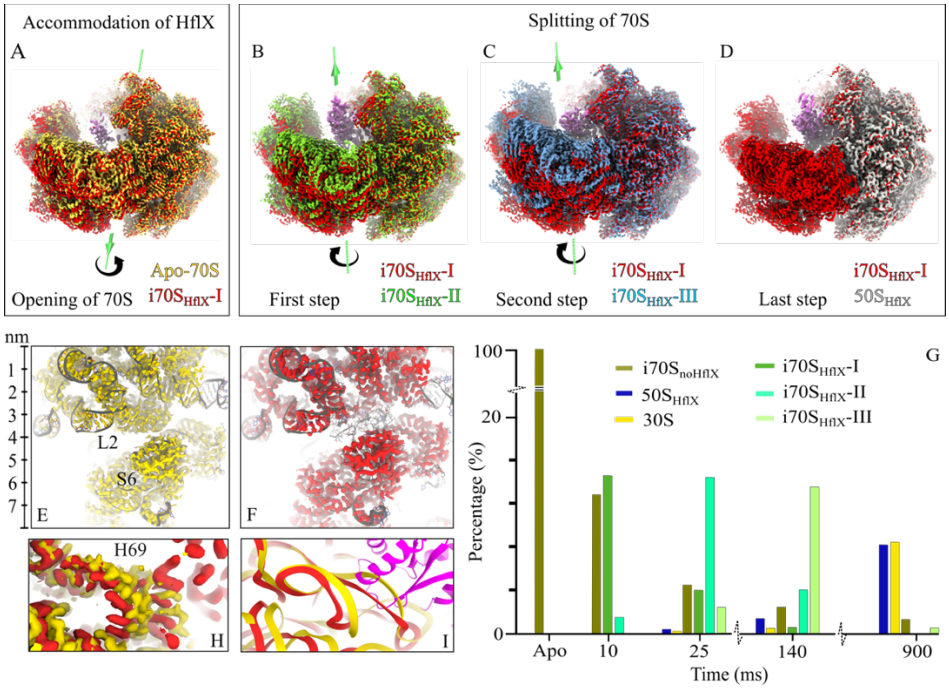

Fig. 1 | Accommodation of HflX on the 70S ribosome and time-dependent 70S splitting: (**A**), Superimposition of reconstructions (Coulomb densities) to show rearrangement of the 30S subunit from apo-70S (yellow) to i70S$_{HflX}$-I (red) to accommodate HflX. The green line represents the initial axis of 30S rotation, Axis I. (**B**) and (**C**), reconstructions of second and third intermediates overlapped with first intermediate, showing the stepwise opening of the 70S by HflX by rotation of the 30S subunit around Axis II (green line). (D), reconstruction of the 50S-HflX complex after the departure of the 30S subunit, overlapped with the first 70S intermediate. In (A) through (D), all reconstructions are aligned on the 50S subunit. (E) and (F), zoomed views of Coulomb densities in yellow for apo-70S and red for i70S$_{HflX}$-I and corresponding atomic models (gray) showing the rearrangement of the intersubunit bridges B7b and B7bR. (**H**) and (**I**), Coulomb densities, and corresponding ribbon models of H69 from apo-70S (yellow), and i70S$_{HflX}$-I (red), respectively, showing the movement of helix H69. HflX is shown in magenta. (**G**) Kinetics of the splitting reaction in terms of the number of particles per class as a function of time, obtained by 3D classification.

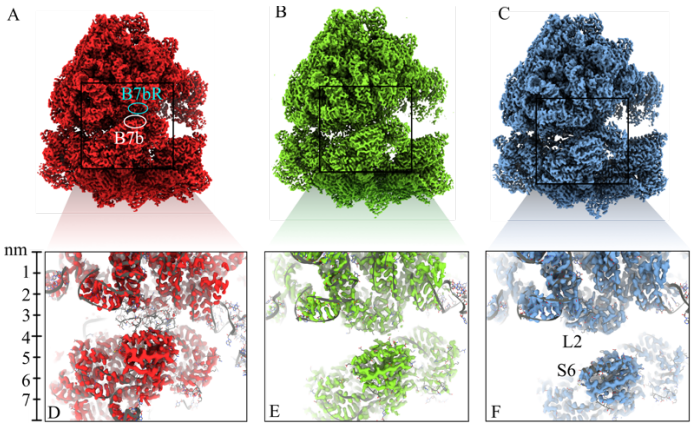

Fig. 2 | Molecular details of subunit interface during the progressive opening of the 70S: (**A**), (**B**), and (**C**), coulomb density maps of intermediates i70S$_{HflX}$-I, i70S$_{HflX}$-II, and i70S$_{HflX}$-III, respectively, in a view showing the separation of the subunits. All maps are aligned on the 50S subunit. (**D**), (**E**), and (**F**), zoomed views showing the time course of splitting of intersubunit bridges B7b and B7bR, and restoration of L2 from disordered (in (**D**) to its original conformation (in (**E**) and (**F**)).

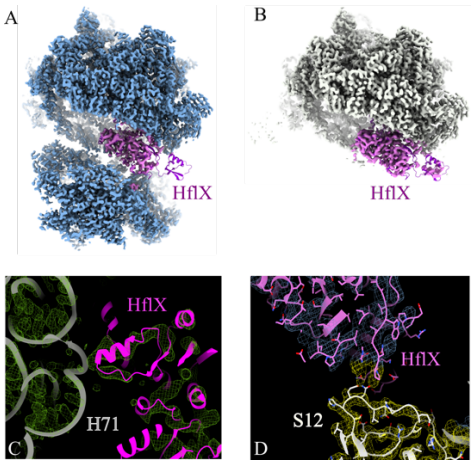

Fig. 3 | Involvement of HflX in 70S splitting. (**A**) Coulomb density of the 70S in i70S$_{HflX}$-III (blue) and associated HflX (magenta) with the fitted atomic model. (**B**) Coulomb density of the final state (gray) showing the 50S subunit with HflX (magenta) along with atomic model. (**C**) Pulling of H71 by the NTD of HflX. (**D**) Pushing of S12 by the HflX GBD flexible loop (E323-G349), leading to dissociation of the 30S subunit from the 70S ribosome.

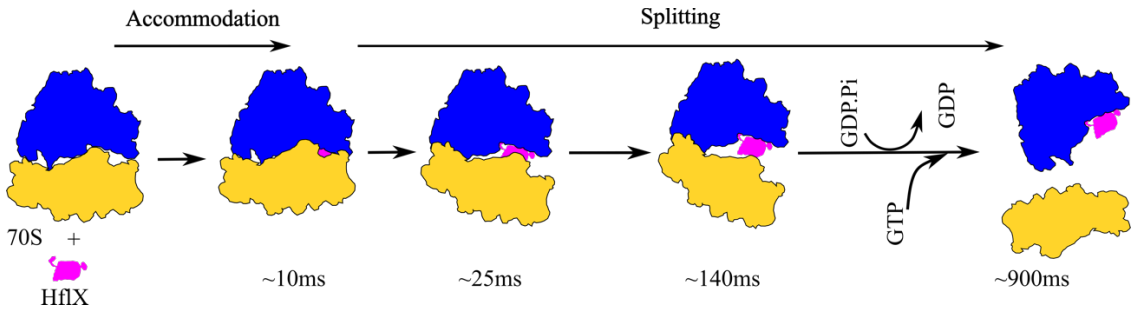

Fig. 4 | Schematic representation of ribosome recycling mechanism. Stepwise splitting of 70S ribosome is shown in the cartoon. The 50S, 30S, and HflX are shown in blue, yellow, and magenta, respectively. The final dissociation of the 30S from 70S occurs after ~140 ms leaving $50S_{HflX}$ as the last state of recycling, where the energy required for a power stroke is set free upon Pi release from GTP·Pi. A new GTP was found to be associated with HflX in the $50S_{HflX}$.

Acknowledgments This work was supported by a grant from the National Institutes of Health R35GM139453 (to J.F.). All data were collected at the Columbia University Cryo-Electron Microscopy Center (CEC). We thank Robert A. Grassucci, Zhening Zhang, and Yen-Hong Kao for their help with the cryo-EM data collection.

Author contributions S.B. conceived the research; S.B., X.F., and J.F. designed the experiments; S.B. prepared the biological samples; X.F. designed the TR chips; S.B. and X.F. performed the TR cryo-EM experiments and data collections; S.B. processed the data; S.M. calculated the subunit and domain motions and the axes of rotation; Z.P.B. helped S.B. with atomic model building and validation, S.B. and J.F. wrote the manuscript with the help of X.F., and S.M. for Methods.

References:

1 Zhang, Y. *et al.* HflX is a ribosome-splitting factor rescuing stalled ribosomes under stress conditions. *Nat Struct Mol Biol* **22**, 906-913 (2015). https://doi.org:10.1038/nsmb.3103

2 Ngan, J. Y. G. *et al.* HflX is a GTPase that controls hypoxia-induced replication arrest in slow-growing mycobacteria. *Proc Natl Acad Sci U S A* **118** (2021). https://doi.org:10.1073/pnas.2006717118

3 Rudra, P., Hurst-Hess, K. R., Cotten, K. L., Partida-Miranda, A. & Ghosh, P. Mycobacterial HflX is a ribosome splitting factor that mediates antibiotic resistance. *Proc Natl Acad Sci U S A* **117**, 629-634 (2020). https://doi.org:10.1073/pnas.1906748117

4 Sengupta, S., Mondal, A., Dutta, D. & Parrack, P. HflX protein protects Escherichia coli from manganese stress. *J Biosci* **43**, 1001-1013 (2018).

5 Wu, H. *et al.* Structure of the ribosome associating GTPase HflX. *Proteins* **78**, 705-713 (2010). https://doi.org:10.1002/prot.22599

6 Coatham, M. L., Brandon, H. E., Fischer, J. J., Schummer, T. & Wieden, H. J. The conserved GTPase HflX is a ribosome splitting factor that binds to the E-site of the bacterial ribosome. *Nucleic Acids Res* **44**, 1952-1961 (2016). https://doi.org:10.1093/nar/gkv1524

7 Verstraeten, N., Fauvart, M., Versees, W. & Michiels, J. The universally conserved prokaryotic GTPases. *Microbiol Mol Biol Rev* **75**, 507-542, second and third pages of table of contents (2011). https://doi.org:10.1128/MMBR.00009-11

8 Basu, A. & Yap, M. N. Disassembly of the Staphylococcus aureus hibernating 100S ribosome by an evolutionarily conserved GTPase. *Proc Natl Acad Sci U S A* **114**, E8165-E8173 (2017). https://doi.org:10.1073/pnas.1709588114

9 Blombach, F. *et al.* An HflX-type GTPase from Sulfolobus solfataricus binds to the 50S ribosomal subunit in all nucleotide-bound states. *J Bacteriol* **193**, 2861-2867 (2011). https://doi.org:10.1128/JB.01552-10

10 Dey, S., Biswas, C. & Sengupta, J. The universally conserved GTPase HflX is an RNA helicase that restores heat-damaged Escherichia coli ribosomes. *J Cell Biol* **217**, 2519-2529 (2018). https://doi.org:10.1083/jcb.201711131

11 Adrian, M., Dubochet, J., Lepault, J. & McDowall, A. W. Cryo-electron microscopy of viruses. *Nature* **308**, 32-36 (1984). https://doi.org:10.1038/308032a0

12 Kaledhonkar, S., Fu, Z., White, H. & Frank, J. Time-Resolved Cryo-electron Microscopy Using a Microfluidic Chip. *Methods Mol Biol* **1764**, 59-71 (2018). https://doi.org:10.1007/978-1-4939-7759-8_4

13 Frank, J. Time-resolved cryo-electron microscopy: Recent progress. *J Struct Biol* **200**, 303-306 (2017). https://doi.org:10.1016/j.jsb.2017.06.005

14 Chen, B. *et al.* Structural dynamics of ribosome subunit association studied by mixing-spraying time-resolved cryogenic electron microscopy. *Structure* **23**, 1097-1105 (2015). https://doi.org:10.1016/j.str.2015.04.007

15 Fu, Z. *et al.* Key Intermediates in Ribosome Recycling Visualized by Time-Resolved Cryoelectron Microscopy. *Structure* **24**, 2092-2101 (2016). https://doi.org:10.1016/j.str.2016.09.014

16 Kaledhonkar, S. *et al.* Late steps in bacterial translation initiation visualized using time-resolved cryo-EM. *Nature* **570**, 400-404 (2019). https://doi.org:10.1038/s41586-019-1249-5

17 Hirokawa, G., Iwakura, N., Kaji, A. & Kaji, H. The role of GTP in transient splitting of 70S ribosomes by RRF (ribosome recycling factor) and EF-G (elongation factor G). *Nucleic Acids Res* **36**, 6676-6687 (2008). https://doi.org:10.1093/nar/gkn647

18 Frank, J. & Agrawal, R. K. A ratchet-like inter-subunit reorganization of the ribosome during translocation. *Nature* **406**, 318-322 (2000). https://doi.org:10.1038/35018597

19 Maji, S., Shahoei, R., Schulten, K. & Frank, J. Quantitative Characterization of Domain Motions in Molecular Machines. *J Phys Chem B* **121**, 3747-3756 (2017). https://doi.org:10.1021/acs.jpcb.6b10732

20 Valle, M. *et al.* Locking and unlocking of ribosomal motions. *Cell* **114**, 123-134 (2003). https://doi.org:10.1016/s0092-8674(03)00476-8

21 Ratje, A. H. *et al.* Head swivel on the ribosome facilitates translocation by means of intra-subunit tRNA hybrid sites. *Nature* **468**, 713-716 (2010). https://doi.org:10.1038/nature09547

22 Borovinskaya, M. A. *et al.* Structural basis for aminoglycoside inhibition of bacterial ribosome recycling. *Nat Struct Mol Biol* **14**, 727-732 (2007). https://doi.org:10.1038/nsmb1271

23 Agrawal, R. K. *et al.* Visualization of ribosome-recycling factor on the Escherichia coli 70S ribosome: functional implications. *Proc Natl Acad Sci U S A* **101**, 8900-8905 (2004). https://doi.org:10.1073/pnas.0401904101

24 Dunkle, J. A. *et al.* Structures of the bacterial ribosome in classical and hybrid states of tRNA binding. *Science* **332**, 981-984 (2011). https://doi.org:10.1126/science.1202692